

Investigation of the magnetic fluctuations in $\text{Tb}_2\text{Sn}_2\text{O}_7$ ordered spin ice by high resolution energy-resolved neutron scattering.

I. Mirebeau¹, H. Mutka², P. Bonville³, A. Apetrei¹, A. Forget³.

¹*Laboratoire Léon Brillouin, CEA-CNRS, CE-Saclay, 91191 Gif-sur-Yvette, France.*

²*Institut Laue Langevin, 6 rue Jules Horowitz, BP 156X, 38042 Grenoble France. and*

³*Service de Physique de l'Etat Condensé, CEA-CNRS, CE-Saclay, 91191 Gif-Sur-Yvette, France.*

We have studied magnetically frustrated $\text{Tb}_2\text{Sn}_2\text{O}_7$ by neutron diffraction and high resolution energy-resolved neutron scattering. At 0.1 K, we observe short range magnetic correlations with a typical scale of 4 Å, close to the near neighbor distance between Tb^{3+} ions. This short range order coexists with ferromagnetic correlations and long range spin ice order at the scales of 18 and 190 Å, respectively. Spin dynamics was investigated at a time scale down to 10^{-9} s, by energy-resolved experiments on a backscattering spectrometer. We observe a freezing of the spin dynamics for all length-scales, with a strong slowing down of the spin fluctuations when long range order settles in. We discuss the spin fluctuations remaining in the ground state in comparison with previous data obtained by muon spectroscopy.

PACS numbers: 71.27.+a, 75.25.+z

Geometrical frustration is expected to favor the onset of unusual types of order such as spin liquid and spin ices, showing a large degeneracy of the magnetic ground state. In spin ices, it leads to non zero ground state entropy akin to that of real ice¹, peculiar freezing dynamics², and short range magnetic orders^{3,4}. Application of a magnetic field lifts the ice rule degeneracy⁵, yielding to excitations which span the entire system⁶, or are akin to magnetic monopoles⁷, depending on the orientation of the field with respect to the anisotropy axis.

Canonical spin ices are observed in pyrochlores $\text{R}_2\text{Ti}_2\text{O}_7$ (R=Dy or Ho), where the rare earth moments occupy a lattice of corner sharing tetrahedra. The stabilization of the spin ice ground state is related to the strong anisotropy of the Dy^{3+} or Ho^{3+} ions, whose moments are constrained to lie along the $\langle 111 \rangle$ local axes connecting the center of each tetrahedron to the summits.

The Tb pyrochlores offer a more complex but even richer behavior, due to the smaller anisotropy of the Tb^{3+} ion, and to the fact that superexchange and dipolar interactions between near-neighbor Tb^{3+} ions nearly compensate. $\text{Tb}_2\text{Sn}_2\text{O}_7$ is an intriguing example of an ordered spin ice⁸. Contrarily to classical spin ices which do not order at large scale, here the four tetrahedra of the unit cell are identical, yielding magnetic Bragg peaks and long range order, at a length scale which increases with decreasing temperature T and reaches about 190 Å at T=0. The onset of this magnetic order is observed at $T_1=1.3(1)$ K. An upturn of the correlation length and magnetic moment, together with a peak in the specific heat, occurs at $T_C=0.87(2)$ K.

Magnetic fluctuations play a prominent role in the ordered spin state of $\text{Tb}_2\text{Sn}_2\text{O}_7$. They were first evidenced by the reduction of the ordered moment as measured using the hyperfine Schottky anomaly of the specific heat and compared with its value from neutron diffraction⁸. Then they were directly observed using μSR ^{9,10}. Surprisingly, no evidence of any static component appears in the local field probed by μSR in spite of the presence

of the magnetic order. The fluctuations of the local field occur at a time scale estimated to either to $8 \cdot 10^{-11}$ s or to $5 \cdot 10^{-9}$ s, depending mostly on the value assumed for the local field^{9,10}. Under applied field, damped oscillations in the muon polarization, and a thermal hysteresis in the longitudinal relaxation rate, show the presence of local configurations frozen at the time scale of the muon probe¹⁰.

Very recently, several inelastic neutron scattering measurements were performed to study the magnetic fluctuations in $\text{Tb}_2\text{Sn}_2\text{O}_7$. Crystal field excitations¹¹ were measured down to 1.4 K and compared to those in $\text{Tb}_2\text{Ti}_2\text{O}_7$, which remains spin liquid down to about 50 mK. It was shown that the wave functions describing the ground and first excited states of the Tb^{3+} ion are exchanged in the two compounds¹¹. However, these differences in the local states of the Tb^{3+} ion cannot explain the different cooperative ground states in the Ti and Sn compounds within the frame of current theories.

Neutron spin echo (NSE) measurements¹² were performed in $\text{Tb}_2\text{Sn}_2\text{O}_7$ for a moment transfer $Q=0.08 \text{ \AA}^{-1}$, outside the Bragg peak positions, probing the dynamics of the ferromagnetic correlations. They clearly observed some spin dynamics down to 0.8 K, but failed to detect any below. Finally, the magnetic cross section was measured by polarized neutrons¹³. The spin dynamics was deduced from the comparison between diffraction measurements (integrating the magnetic signal over all energies up to 3 meV) and elastic scattering with a coarse energy resolution (integration over an energy window of ± 0.15 meV). At 0.04 K, the authors conclude to the presence of static Bragg peaks, together with a liquid-like structure factor arising from spins moving faster than 0.04 THz.

Here we have investigated the spin correlations and dynamics in $\text{Tb}_2\text{Sn}_2\text{O}_7$ by combining neutron diffraction and energy resolved neutron scattering measurements, with a very high energy resolution of $0.5 \mu\text{eV}$ at half width half maximum, probing time scales up to 1.3

10^{-9} s. Both measurements were performed in the temperature range 0.1 K-1.4 K. The Q and T dependence of the magnetic scattering was analyzed quantitatively, considering not only the Bragg scattering, but also the medium and short range correlations. Diffraction data measured at 0.1 K show the coexistence of several length scales, corresponding to first neighbors (~ 4 Å), medium (18 Å), and long range (190 Å) correlations. The spin dynamics was investigated in different Q ranges where either short or long length scales are dominant. When T decreases, we observe a freezing of the spin dynamics for all length scales, with a stronger effect in the region of the transition. Some spin fluctuations persist down to the lowest temperature of 0.1 K. We discuss these results with respect to the fluctuations in the ground state in $\text{Tb}_2\text{Sn}_2\text{O}_7$.

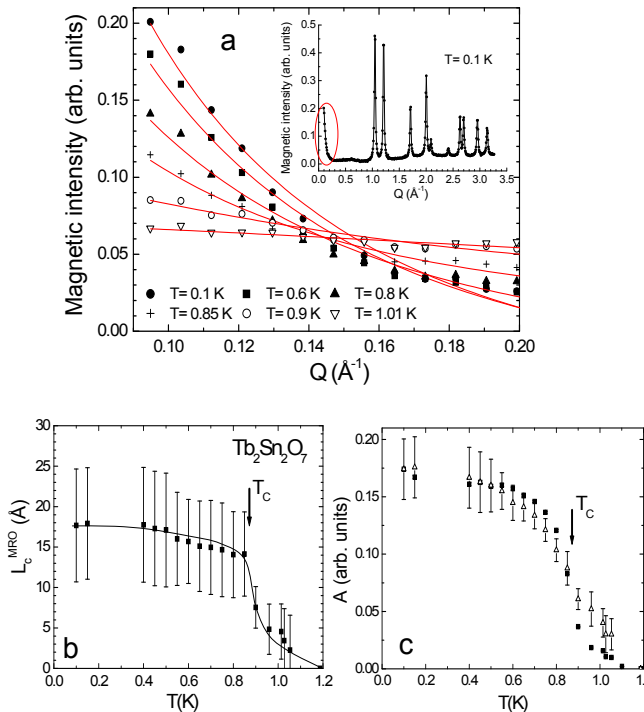


FIG. 1: (Colour online) a: Magnetic intensity measured $\text{Tb}_2\text{Sn}_2\text{O}_7$ by neutron diffraction at small angles, versus the momentum transfer Q for several temperatures. A spectrum above 1.2 K was subtracted. Solid lines are Lorentzian fit (see text). In inset, the total diffraction pattern at 0.1 K showing the small angle intensity together with the magnetic Bragg peaks. b: medium correlation length $L_c^{\text{MRO}} = 1/\kappa$ (full squares) versus temperature T . The solid line is a guide to the eye. c: norm A of the Lorentzian (open triangles) and intensity of the magnetic Bragg peaks (full squares) versus temperature.

I. NEUTRON DIFFRACTION

Neutron diffraction measurements were performed on the D1B spectrometer at the Institut Laue Langevin

(ILL) with an incident neutron wavelength of 2.52 Å. The magnetic long range order was already studied in ref. 8 from the same data. The magnetic cross section was isolated by subtracting a spectrum measured at 1.2 K. The magnetic diffraction pattern at 0.1 K (inset Fig 1a) shows an intense small angle neutron scattering (SANS) signal for $Q < 0.2 \text{ \AA}^{-1}$, arising from ferromagnetic correlations. The SANS signal (Fig. 1a) strongly increases with decreasing T , and flattens in the range of the transition. It was fitted by a Lorentzian function $I(Q) = \frac{A}{\pi} \frac{\kappa}{\kappa^2 + Q^2}$. Good fits are obtained down to about 0.6 K, but the fit quality decreases below. The fit however allows one to estimate the medium correlation length $L_c^{\text{MRO}} = 1/\kappa$ (Fig. 1b) versus temperature in the ordered region. With decreasing temperature, L_c^{MRO} increases from values close to the near neighbor distance between Tb^{3+} moments ($d=3.686$ Å), to about 18(6) Å below 0.8 K. This value is about 10 times smaller than that deduced from the width of the magnetic Bragg peaks ($L_c=190$ Å as shown in ref. 8) but its temperature dependence is quite similar. The parameter A increases with decreasing temperature. Its variation compares well with that of the LRO squared magnetic moment deduced from the Bragg peak intensity, although it is less sharp in the transition region (Fig. 1c).

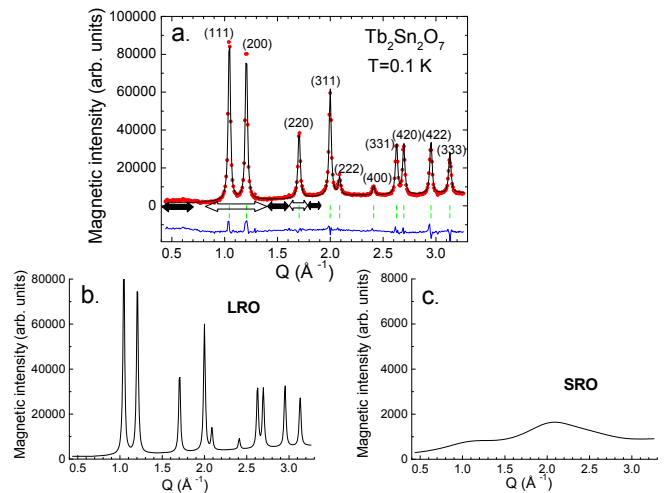


FIG. 2: (Colour online) a: Magnetic diffraction spectrum of $\text{Tb}_2\text{Sn}_2\text{O}_7$ versus the momentum transfer Q at 0.1 K. A spectrum taken into account both LRO and SRO contributions. A linear background is also added. The arrows correspond to the Q -bands selected in the time-resolved experiment. White arrows correspond to the Bragg Q -bands, black arrows to the low, medium and high Q -bands; b: (resp c:) calculated LRO (resp. SRO) contribution to the diffraction pattern.

The short range order (SRO) yields a diffuse magnetic scattering which remains clearly visible at 0.1 K. This scattering was not analyzed in ref. 8. Here we refined it as a magnetic structure, assuming that it has the same symmetry as the LRO, but a much shorter correlation length. The relative contributions of the SRO and LRO

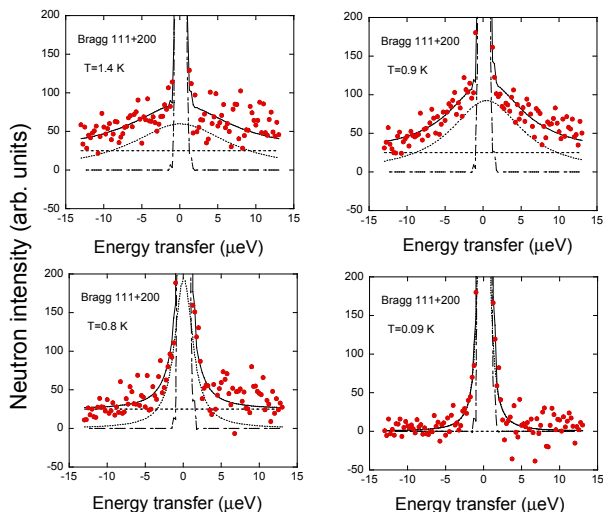


FIG. 3: (Colour online) Inelastic neutron spectra of $\text{Tb}_2\text{Sn}_2\text{O}_7$ for several temperatures measured in the Q -range of the 111 and 200 Bragg peaks. The solid line is a fit as described in the text. Dotted, dashed-dotted and dashed lines correspond to the quasielastic, elastic and flat "background" terms respectively.

are shown in Fig. 2. From the fit, we obtain values of LRO and SRO moments of $5.8(1)$ and $3.3(3) \mu_B$ respectively. The value of the LRO moment, ordered at the scale of 190 \AA deduced from the width of the Bragg peaks, agree with the value previously determined of $5.9(1) \mu_B$. The SRO moment compares well with the value of about $3 \mu_B$ obtained by calibration of the diffuse magnetic scattering measured with polarized neutrons¹³. This analysis shows that a large amount of the Tb^{3+} moments remains ordered at a very short length scale, estimated here to $4(1) \text{ \AA}$ from the refinement, therefore comparable to the distance between first neighbor Tb^{3+} moments (3.686 \AA). Assuming that both types of correlations contribute to the neutron intensity independently, we estimate the total ordered moment to $M = 6.6(2) \mu_B / \text{Tb}$. We notice that this value is exactly the value calculated for the total local moment within the crystal field model (Fig. 15 of ref. 11).

The above analysis shows the presence of three characteristic length scales for the spin correlations at low temperature, with values ranging from the first neighbor distance to length scales of about 18 cubic unit cells (the lattice constant $a = 10.426 \text{ \AA}$). A distribution of length scales was previously inferred from an independent analysis of the profile peak shape¹².

II. ENERGY RESOLVED NEUTRON SCATTERING

The analysis above motivates a study of the slow spin dynamics at different Q -ranges, where either short or long length scales dominate. For this purpose we per-

formed energy resolved neutron scattering measurements on the IN16 backscattering spectrometer of the ILL, with an incident neutron wavelength of 6.27 \AA . This instrument offers a dynamic range of $\pm 15 \mu\text{eV}$ for the observation of fluctuations characterized by a quasielastic response. Due to the large angular acceptances of the backscattering method the wave-vector transfer resolution is rather relaxed, anyhow sufficient to discriminate regions of interest with or without contributions from the Bragg peaks associated with the long-range ordering process. Optionally one can switch off the energy transfer analysis to follow only the elastic response within the resolution window of $1 \mu\text{eV}$ at full width half maximum (FWHM). Accordingly one can obtain a temperature scan of the elastic contribution over the whole Q -range and compare intensity in specific Q -bands to the temperature variation observed for the Bragg peaks in the diffraction experiment.

The sample was packed in a 1 mm thick flat can in order to minimize the sample absorption. The transmission was evaluated to 0.9. The counting time was 12 hours for each temperature. A vanadium sample of the same shape was measured to calibrate the angle dependent detection efficiency and determine the energy resolution.

The spectra were corrected for background and absorption using spectra of the empty sample holder measured in the same conditions, taking into account the specific corrections due to the backscattering geometry¹⁴. Temperature scan of the elastic resolved scattering was taken in the range $0.1 \leq T < 1.4 \text{ K}$. The quasielastic spectra were recorded in a range $0.1 < Q < 1.9 \text{ \AA}^{-1}$. They were grouped into five Q -bands, three bands out of the Bragg peaks, and two at the Bragg peak positions. The Q -bands outside the Bragg peaks are respectively called the low Q -band, ($Q = 0.55 \pm 0.15 \text{ \AA}^{-1}$), the medium Q -band ($Q = 1.5 \pm 0.1 \text{ \AA}^{-1}$) and the high Q -band ($Q = 1.85 \pm 0.05 \text{ \AA}^{-1}$). The Q -bands at the Bragg peak positions are respectively $Q_{111+200} = 1.1 \pm 0.3 \text{ \AA}^{-1}$ and $Q_{220} = 1.7 \pm 0.1 \text{ \AA}^{-1}$, the first for the 111 and 200 together (not well resolved individually) and the second for 220 contribution. The 311 Bragg peak is out of the accessible Q -range. We have situated these Q -bands in the diffraction pattern of the Fig. 2. One sees that the Bragg Q -bands mostly probe the long length scales (the Bragg intensity dominates), whereas the low, medium and high- Q bands probe the shortest lengthscale. We also note that the nuclear Bragg contribution on all of the above peaks is either zero or negligible, and that the overall nuclear incoherent contribution is also small due to the small incoherent cross-sections of the elements. By fitting the vanadium patterns with a Gaussian function, we get an energy resolution at half width half maximum (HWHM) of $0.4 \mu\text{eV}$ in the Bragg peak and large angle regions, and $0.55 \mu\text{eV}$ in the low angle region.

Typical energy resolved neutron scattering patterns are shown in Fig. 3, in the Q -band covering the 111 and 200 Bragg peaks. They clearly show a quasi-elastic signal in the temperature range 0.8-1.2 K. The quasielastic sig-

nal strongly narrows with decreasing temperature, which reflects the freezing of the spin dynamics around the transition. The neutron intensity was fitted by the sum of three contributions. First, an elastic (or resolution-limited) signal of intensity C_1 , of magnetic origin mostly, accounts for the spins which fluctuate at time scales longer than the resolution limit. Second, a Lorentzian function of intensity C_2 and half-width at half maximum (HWHM) Γ accounts for the quasi elastic signal. The Lorentzian quasi elastic signal was convoluted by the instrumental resolution. An energy-independent flat level "background" C_B accounts for the "fast" fluctuations (or short time scales), corresponding to energy widths larger than the energy window. Above 1 K, the flat level and the rather broad Lorentzian contributions cannot be determined independently with good accuracy. So, the value of C_B was fixed to the value at 0.9 K. Below 0.6 K, the quasielastic linewidth has the same order of magnitude as the resolution, and the flat level vanishes.

The parameters deduced from the fits are plotted versus temperature in Fig. 4 in the Q -band of the 111 and 200 Bragg peaks. Similar results are obtained for the Q -band of the 220 peak. The elastic intensity C_1 increases with decreasing T . Its temperature variation scales quite well with that of the Bragg intensity deduced from diffraction data. The latter represents a constant angle integral of the scattering cross-section over energy transfers up to the incident neutron energy (inset Fig. 4). Just below $T_C=0.87(2)$ K, the intensity measured by diffraction increases more sharply with decreasing T than the elastic intensity. The differences in the T -dependence of the Bragg peak and the elastic resolved intensities can be explained by two factors, one being the possibility of integrating the "fast" dynamics (represented by the flat level in the energy resolved experiment), the other the coarser Q -resolution of the time resolved patterns, which integrate a contribution from the SRO not included in the Bragg peaks of the diffraction patterns.

The quasielastic intensity C_2 shows a broad maximum in the transition region, where the contribution from the fast fluctuations starts to enter the energy window. As T decreases further, C_2 starts to decrease when the spectral weight is transferred to the elastic intensity. The energy width 2Γ decreases rapidly down to 0.8 K; a quasielastic signal of width close to the resolution limit remains at 0.09 K. The energy independent flat level C_B also decreases with decreasing temperature. At 0.09 K, there is no visible contribution of the "fast" fluctuations to the energy pattern and C_B was fixed to zero.

The temperature variations of the parameters C_1 , C_2 , C_B and Γ reflect a freezing of the spin dynamics. The elastic contribution increases at the expense of the "fast" fluctuations and quasielastic contributions, whereas the decrease of the linewidth reflects the increase of the relaxation time probed in the time window of the measurement.

The Lorentzian line shape of the quasielastic signal corresponds to a relaxation process which involves spin fluctua-

tions with a lifetime τ ($\langle S(0) \cdot S(t) \rangle \propto e^{-t/\tau}$). Taking the Fourier transform of this expression yields $\tau = \hbar/\Gamma$, where $\hbar = 0.658 \cdot 10^{-9} \mu\text{eV} \cdot \text{s}$ (see note 15). The T dependence of the relaxation time is shown in Fig. 4 c. At 0.09 K, the time scale of the spin fluctuations is equal to $\tau_0 = 1.3 \cdot 10^{-9} \text{ s}$ ($\Gamma = 0.5 \mu\text{eV}$).

Energy spectra in the low, medium and high Q -bands also probe a freezing of the spin dynamics. Here, no contribution of a flat level was detected and the fits were performed with C_1 and C_2 contributions only. Their variations (Fig. 5) reflect those at the magnetic Bragg peaks. The Γ values at 0.09 K are higher, probing fluctuations at shorter time scales ($\tau_0 \sim 0.3\text{-}1 \cdot 10^{-9} \text{ s}$). The relative weight of the "fluctuating" spins with respect to the "static" spins at low temperature is also higher in the Q -bands outside the Bragg peaks. Here the terms "static" and "fluctuating" refer to the time scale defined by the instrumental resolution of IN16 ($1.3 \cdot 10^{-9} \text{ s}$) and sensitivity of the fit.

One notices that due to the limited time window and the strong change of the correlations with temperature, the opposite variations of the quasielastic and elastic intensities during the freezing process do not compensate in a given Q -band. Namely, at the Bragg peaks the "loss" in the quasielastic intensity with decreasing temperature is much smaller than the "gain" in the elastic intensity, whereas the reverse situation occurs outside the Bragg peaks.

III. DISCUSSION

The above features show a distribution of time scales, which extends to longer times with decreasing temperature, as the characteristic length scales of the spin correlations increase. Somewhat similar effects are seen in other frustrated magnets. A distribution of fluctuation times concomitant with a distribution of correlation lengths is observed by neutron scattering in disordered systems such as spin glasses^{16,17}. A broad range of time scales in absence of long-range order but with remarkably energy(time)-scale invariant short-ranged correlations was also seen in the well-known geometrically frustrated Kagome spin system SCGO¹⁸.

The time scale of the fluctuations is in rather good agreement with the time scale probed by neutron spin echo (NSE) experiment¹² in the range of the transition ($\tau \sim 0.2 \cdot 10^{-9} \text{ s}$ for $T=0.8 \text{ K}$ and $Q=0.08 \text{ \AA}^{-1}$). At 0.1 K, when NSE did not observe further dynamics, our experiment in the backscattering geometry still suggests fluctuations at a time scale τ_0 with τ_0 ranging from 1.3 to $0.3 \cdot 10^{-9} \text{ s}$, the shortest time scales corresponding to the SRO. Fluctuations at longer time scales than τ_0 do exist (the elastic scattering), but no faster fluctuations are probed (there is no residual background in the energy window).

The life time of the spin fluctuations may be compared to that probed by μSR experiments^{9,10}. In ref. 10, the

μ SR response was interpreted by a relaxation process between different configurations of the local field B_{loc} . The typical time τ_c of this process can be evaluated from the longitudinal relaxation rate λ_Z by the relation $\tau_c \sim \lambda_Z / (\gamma_\mu B_{loc})^2$ where γ_μ is the muon gyromagnetic ratio. At 0.1 K τ_c could be evaluated to $8 \cdot 10^{-11}$ s in ref. 9 (taking $B_{loc}=0.2$ T) and $5 \cdot 10^{-9}$ s in ref. 10 (taking $B_{loc}=0.02$ T). Our estimation of the life time ($\tau_0 \sim 0.3-1.3 \cdot 10^{-9}$ s) situates in between these values.

On the other hand, the fluctuations at longer time scales than τ_0 , clearly seen by neutrons (they give rise to the elastic scattering and to a static response in the NSE experiment), do not yield any static component in the muon spectra. A strong fully static component cannot be excluded by the neutron data, but seems to be incompatible with the muon ones. To investigate this point further, we computed the muon depolarization in presence of a dipolar field randomly reversing with the frequency ν , as done in ref. 19. This shows that fluctuations with a frequency $\nu > 2\gamma_\mu B_{loc}$ should wash out the precession signal, clear-cut signature of a static field in the muon data. For $B_{loc}=0.02$ T, this yields a higher limit of $2 \cdot 10^{-8}$ s for the typical time scale $\tau=1/\nu$ of the fluctuations¹⁵, which is still compatible with the lower limit of $1.3 \cdot 10^{-9}$ s given by the instrumental resolution of IN16. This is no longer true for the higher value $B_{loc}=0.2$ T. Comparison between muon and neutron data therefore favor a lower estimation of the internal field.

The fluctuations of the local field in ordered spin ice $Tb_2Sn_2O_7$ found by μ SR found by are quite similar to those observed in the parent spin liquid $Tb_2Ti_2O_7$. In both compounds, the short scale fluctuations may involve tunnelling or thermally activated excitations between the six degenerated configurations of the spin ice structure. In ordered $Tb_2Sn_2O_7$, such excitations may also help to "switch" domains of longer length scales.

In $Tb_2Sn_2O_7$, our results suggest a homogeneous picture where different correlation lengths involve differ-

ent spin components and different time scales, rather than a coexistence of independent clusters with different sizes. In the pyrochlore spinel $ZnCr_2O_4$ and related compounds, a cluster-like scattering process has been invoked, with the presence of emergent excitations within loops of strongly bound hexagonal clusters²⁰. More recently however, theoretical work on the "true" spin ice $Dy_2Ti_2O_7$ showed that this picture does not necessarily imply real independent clusters and that long range interactions are relevant²¹. Whether such picture can be extended to describe excitations in the ground state of the ordered spin ice $Tb_2Sn_2O_7$, in which we observed multiple length scales, remains a matter for further theories.

IV. CONCLUSION

In conclusion, in $Tb_2Sn_2O_7$ ordered spin ice we have observed a freezing of the spin fluctuations which involves the coexistence of different correlations lengths and times scales. The distribution extends to longer times with decreasing temperature. A marked slowing down is observed in the transition region, in agreement with previous muon and neutron spin echo experiments. At the lowest temperature, the time scale of the spin fluctuations ranges between 1.3 and $0.3 \cdot 10^{-9}$ s. Fluctuations at longer time scales are also observed by neutrons, whereas they give no clear-cut signature in the muon spectra. This may be compatible with the low estimation of the local field ($B_{loc}=0.02$ T) found in μ SR. The presence of multiple time scales remains to be understood in further theoretical work.

We thank B. Frick and R. Chung for the help with the back scattering neutron experiment, O. Isnard for the help with the neutron diffraction experiment, and J.-L. Ragazzoni for setting up the dilution equipment.

¹ A. P. Ramirez, A. Hayashi, R.J. Cava, R. Siddhant, B. S. Shastry, Nature **399**, 333 (1999).

² J. Snyder, J.S. Slusky, R.J. Cava, P. Schiffer, Nature **413**, 48 (2001).

³ S.T. Bramwell, M.J. Harris, B.C. den Hertog, M.J.P. Gingras, J.S. Gardner, D.F. McMorrow, A.R. Wildes, A. Cornelius, J.D.M. Champion, R.G. Melko, T. Fennell Phys. Rev. Lett. **87**, 047205 (2001).

⁴ S.T. Bramwell, M.J.P. Gingras Science **294**, 1495 (2001).

⁵ H. Fukazawa, R.G. Melko, R. Higashinaka, Y. Maeno, M.J.P. Gingras, Phys. Rev. B. **65**, 54410 (2002).

⁶ L.D.C. Jaubert, J.T. Chalker, P.C.W. Holdsworth, R. Moessner Phys. Rev. Lett. **100**, 67207 (2008).

⁷ C. Castelnovo, R. Moessner, S.L. Sondhi, Nature **451**, 42 (2008).

⁸ I. Mirebeau, A. Apetrei, J. Rodriguez-Carvajal, P. Bonville, A. Forget, D. Colson, V. Glazkov, J.P. Sanchez, O. Isnard and E. Suard, Phys. Rev. Lett. **94**, 246402

(2005).

⁹ P. Dalmas de Réotier, A. Yaouanc, L. Keller, A. Cervellino, B. Roessli, C. Baines, A. Forget, C. Vaju, P.C.M. Gubbens, A. Amato, P.J.C. King, Phys. Rev. Lett. **96**, 127202 (2006).

¹⁰ F. Bert, P. Mendels, A. Olariu, N. Blanchard, G. Collin, A. Amato, C. Baines and A.D. Hillier, Phys. Rev. Lett. **97**, 117203 (2006).

¹¹ I. Mirebeau, P. Bonville, M. Hennion Phys. Rev. B. **76**, 184436 (2007).

¹² Y. Chapuis, A. Yaouanc, P. Dalmas de Réotier, S. Pouget, P. Fouquet, A. Cervellino, A. Forget, J. Phys. Cond. Mat. **19**, 446206 (2007).

¹³ K.C. Rule, G. Ehlers, J.R. Stewart, A.L. Cornelius, P.P. Deen, Y. Qiu, C. R. Wiebe, J.A. Janik, H.D. Zhou, D. Antonio, B.W. Woytko, J. P. Ruff, H.A. Dabkowska, B.D. Gaulin and J.S. Gardner Phys. Rev. B. **76**, 212405 (2007).

¹⁴ O.G. Randl, ILL report 96RA07T (1996).

- ¹⁵ The equation which yields the typical time scale holds because it involves an *energy* measurement and a Fourier transform. This is the case for Quasielastic or Inelastic Neutron Scattering, Electronic Paramagnetic Resonance, Mössbauer spectroscopy or energy-resolved Nuclear Magnetic Resonance (NMR). The time involved results from a dynamical broadening or from the peak lineshape associated with the physical process, so that the characteristic time is the inverse of the pulsation ω , namely $\tau = 1/\omega = 1/2\pi\nu$, where ν is the frequency equivalent to the energy $\hbar\omega$ involved in the process. On the reverse, when the typical time scale is determined from a *time* measurement such as muon spectroscopy or time-resolved NMR, where the process involved is expressed as $e^{-t/\tau}$, then $\tau = 1/\nu$ is expressed as the inverse of the frequency. This is also the case when τ is simply *defined* with respect to the frequency of a physical event, as being the average time between two events.
- ¹⁶ A.P. Murani, J. Phys. F: Met. Phys., **15**, 417 (1985).
- ¹⁷ C. Bellouard, M. Hennion, I. Mirebeau and B. Hennion, J. Mag. Mag. Mat., **104-107**, 1627 (1997).
- ¹⁸ C. Mondelli, H. Mutka, B. Frick, C. Payen, Physica B, **266**, 104-107 (1999); H. Mutka, G. Ehlers, C. Payen, D. Bono, J.R. Stewart, P. Fouquet, P. Mendels, J.Y. Mevellec, N. Blanchard, G. Collin, Phys. Rev. Lett. **97**, 047203 (2006).
- ¹⁹ P. Bonville, I. Mirebeau, J.-P. Sanchez, CP1003, ICMM-2007 <http://proceedings.aip.org/proceedings/cpcr.jsp>
- ²⁰ S.-H. Lee, C. Broholm, W. Ratcliff, G. Gasparovic, Q. Huang, T.H. Kim, S.-W. Cheong Nature **418**, 856 (2002).
- ²¹ T. Yavors'kii, T. Fennell, M.J.P. Gingras, S. T. Bramwell Phys. Rev. Lett. **101**, 037204 (2008).

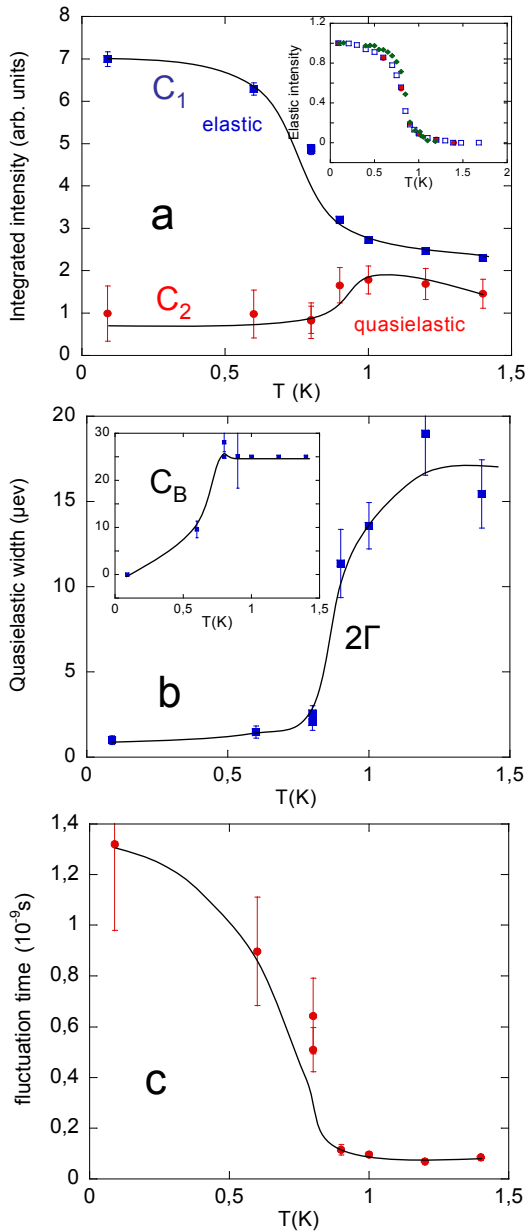


FIG. 4: (Colour online) Temperature dependence of the parameters deduced from the fit of the inelastic spectra in the region of the 111 and 200 Bragg peaks. a: elastic intensity C_1 and quasielastic intensity C_2 deduced from the fit of the energy patterns. In inset: the elastic intensity (full dots) is compared to the intensity from elastic scans (open squares) and to the integrated intensity of a magnetic Bragg peak measured in diffraction (diamonds). All quantities are scaled to vary between 1 at 0.1 K and 0 at 1.4 K. b: quasielastic width 2Γ versus temperature. In inset: the background level C_B , involving fluctuations at a shorter time scale than probed in the energy window. c: the fluctuation time $\tau = \hbar/\Gamma$. Solid lines are guides to the eye.

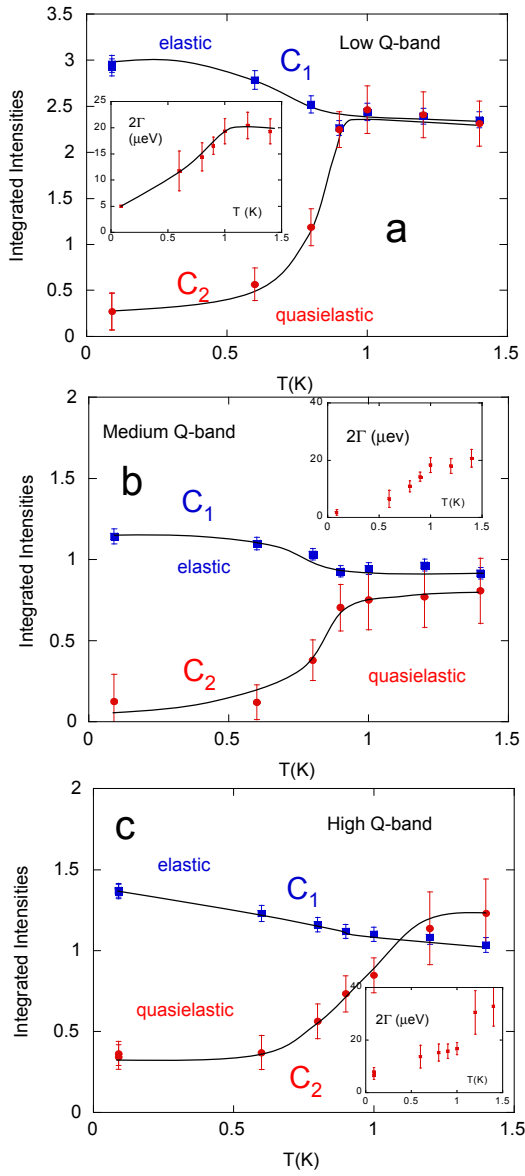


FIG. 5: (Colour online) Temperature dependence of the integrated elastic and quasi elastic intensities. The background level was fixed to zero at all temperatures. Solid lines are guides to the eye. Fig. 5a, 5b, and 5c correspond to low, medium and high Q -bands respectively. In the insets: the quasielastic width 2Γ versus temperature. The width at 0.09 K in the inset of Fig. 5a was fixed.